Science of the Total Environment 831 (2022) 154905

Contents lists available at ScienceDirect

Science of the Total Environment

journal homepage: www.elsevier.com/locate/scitotenv

Air-water interfacial adsorption of C4-C10 perfluorocarboxylic acids during transport in unsaturated porous media

Ying Lyu [a,b,c,*], Baohua Wang [a,b], Xinqiang Du [a,b], Bo Guo [d], Mark L. Brusseau [d,e,**]

[a] Key Lab of Groundwater Resources and Environment, Ministry of Education, Jilin University, Changchun 130026, PR China
[b] Jilin Provincial Key Laboratory of Water Resources and Environment, Jilin University, Changchun 130026, PR China
[c] Institute of Water Resources and Environment, Jilin University, Changchun 130026, PR China
[d] Department of Hydrology and Atmospheric Sciences, University of Arizona, 429 Shantz Bldg., USA
[e] Department of Environmental Science, University of Arizona, 429 Shantz Bldg., USA

HIGHLIGHTS

- Transport of PFCAs in an unsaturated porous medium was investigated.
- The magnitude of air–water interfacial adsorption correlated to PFCA chain length
- Air-water interfacial adsorption was of lesser significance for shorter-chain PFCAs.
- The importance of nonlinear air–water interfacial adsorption varied by PFCA

GRAPHICAL ABSTRACT

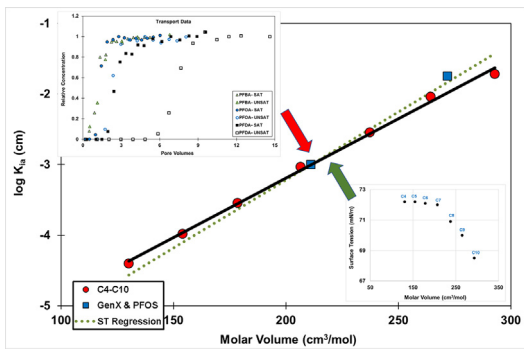

ARTICLE INFO

Article history:
Received 21 December 2021
Received in revised form 23 March 2022
Accepted 25 March 2022
Available online 30 March 2022

Editor: Damià Barceló

Keywords:
PFCAs
PFAS
Air-water interfacial adsorption
Chain length
Sorption
Retention

ABSTRACT

The impact of chain length on air-water interfacial adsorption of perfluorocarboxylic acids (PFCAs) during transport in unsaturated quartz sand was investigated. Short-chain (C4-C7: PFBA, PFPeA, PFHxA, PFHpA) and long chain (C8-C10: PFOA, PFNA, PFDA) PFCAs were selected as a representative homologous series. Surface tensions were measured to characterize surface activities of the selected PFCAs. Miscible-displacement column experiments were conducted for each of the PFCAs to characterize the magnitudes of air–water interfacial adsorption under transport conditions. The transport of the long-chain PFCAs exhibited greater retardation than the short-chain PFCAs. Air–water interfacial adsorption (AWIA) was the predominant source of retention (≥63%) for the long-chain PFCAs. Conversely, AWIA contributed less to retention than did solid-phase sorption for the short-chain PFCAs, with the former contributions ranging from 4% to 40%. Direct examination of the breakthrough-curve profiles as well as mathematical-modeling results demonstrated that transport of the two longest-chain PFCAs was influenced by nonlinear AWIA, whereas that of the shorter-chain PFCAs was not. This disparate behavior is consistent with the input concentration used for the transport experiments in comparison to the respective surface activities and critical reference concentrations of the different PFCAs. Quantitative-structure/property-relationship (QSPR) analysis was applied to characterize the influence of molecular size on air-water interfacial adsorption. The logs of the air-water interfacial adsorption coefficients (K_{ia}) determined from the transport experiments are a monotonic function of molar volume, consistent with prior QSPR analyses of surface-tension measured values. The K_{ia} values determined from the transport experiments are very similar to those measured from surface-tension data, indicating that the transport experiments produced robust measurements of AWIA.

* Corresponding author at: Key Lab of Groundwater Resources and Environment, Ministry of Education, Jilin University, Changchun 130026, PR China.
** Corresponding author at: Department of Environmental Science, University of Arizona, 429 Shantz Bldg., USA.
E-mail addresses: yinglyu@jlu.edu.cn (Y. Lyu), brusseau@arizona.edu (M.L. Brusseau).

http://dx.doi.org/10.1016/j.scitotenv.2022.154905
0048-9697/© 2022 Elsevier B.V. All rights reserved.

1. Introduction

Per- and poly-fluoroalkyl substances (PFAS) are emerging global contaminants of critical concern. PFAS are present in soil and groundwater across the world (Rayne and Forest, 2009; Ahrens, 2011; Backe et al., 2013; Krafft and Riess, 2015; Anderson et al., 2016; Cousins et al., 2016; Rankin et al., 2016; Hatton et al., 2018; Brusseau et al., 2020a). Recent research has demonstrated that soil can serve as a long-term reservoir of PFAS at many sites (e.g., Xiao et al., 2015; Weber et al., 2017; Brusseau et al., 2020a). As such, there is great interest in understanding the transport behavior of PFAS in unsaturated porous media, and the factors and processes that influence retention.

Numerous laboratory studies have demonstrated that sorption by soils and sediments is generally a significant source of retention for PFAS, the specific degree to which depending upon the properties of the PFAS and medium. The transport of PFAS in soil and the vadose zone can be influenced by an additional retention process, namely adsorption at air-water interfaces (Brusseau, 2018). The impact of air–water interfacial adsorption on PFAS transport in unsaturated media has been demonstrated recently by the results of miscible-displacement experiments conducted with water-unsaturated systems (Lyu et al., 2018; Brusseau et al., 2019a; Lyu and Brusseau, 2020; Lyu et al., 2020; Yan et al., 2020; Brusseau et al., 2021; Li et al., 2021). The results of these experiments show that air–water interfacial adsorption can contribute significantly, and in some cases predominantly, to overall retention depending upon the specific PFAS, porous medium, and environmental conditions. The significance of air–water interfacial adsorption for PFAS transport in the vadose zone has been illustrated in recent mathematical-modeling studies (Guo et al., 2020; Silva et al., 2020; Zeng and Guo, 2021; Zeng et al., 2021).

PFAS comprise hydrophobic/oleophobic fluoroalkyl groups of different chain lengths. The transport and fate behavior of PFAS is known to be a function in part of chain length, including the magnitude of solid-phase sorption (e.g., Higgins and Luthy, 2006; Guelfo and Higgins, 2013; Milinovic et al., 2015; Anderson et al., 2016; Campos Pereira et al., 2018; Brusseau, 2019b; Nguyen et al., 2020), surface activity (e.g., Lunkenheimer et al., 2015), and air-water interfacial adsorption (e.g., Brusseau, 2019a; Brusseau and Van Glubt, 2021). While the impact of chain length on air-water interfacial adsorption of PFAS has been investigated in surface-tension-based studies, the few unsaturated-flow transport experiments conducted to date have focused primarily on a single PFAS and have not compared the air–water interfacial adsorption of PFAS as a function of chain length. In addition, the few studies that have examined the transport of different chain-length hydrocarbon surfactants under unsaturated conditions either did not discuss air-water interfacial adsorption (Miller and Letey, 1975; Mingorance et al., 2007) or did not quantify its individual contribution to retention (Allred and Brown, 1996; Allred and Brown, 2001). Hence, to the best of our knowledge, the specific impact of chain length on air–water interfacial adsorption and retention of PFAS or hydrocarbon surfactants in unsaturated porous media has not yet been investigated under dynamic transport conditions via miscible-displacement experiments.

The objective of this research is to examine the impact of chain length on air-water interfacial adsorption of PFAS during transport in unsaturated porous media. Short-chain (C4-C7: PFBA, PFPeA, PFHxA, PFHpA) and long chain (C8-C10: PFOA, PFNA, PFDA) PFCAs are selected as a representative homologous series of PFAS. Surface tensions are measured to characterize surface activity of the selected PFCAs. Miscible-displacement transport experiments are conducted under saturated and unsaturated conditions to characterize the magnitude of solid-phase sorption and air-water interfacial adsorption, respectively. Direct analysis of breakthrough-curve and elution-front profiles is used to assess the potential influence of non-equilibrium and non-linear air-water interfacial adsorption. PFCA transport is simulated using a mathematical model that accounts for surfactant-induced flow, nonlinear, rate-limited solid-phase sorption, and nonlinear, rate-limited air-water interfacial adsorption. Quantitative-structure/property-relationship (QSPR) analysis is applied to characterize the influence of molecular size on air–water interfacial adsorption.

2. Materials and methods

2.1. Materials

The C4-C10 homologous series of perfluorocarboxylic acids (PFCAs) was selected as representative short-chain and long-chain PFAS. The standardized nomenclature for chain length is employed, with $n < 7$ fluorinated carbons defined as short-chain PFCAs (Buck et al., 2011). Perfluorobutanoic acid (PFBA, $C_4HF_7O_2$, CAS#375-22-4; 98% purity), Perfluoropentanoic acid (PFPeA, $C_5HF_9O_2$, CAS# 2706-90-3; 97% purity), Perfluorohexanoic acid (PFHxA, $C_6HF_{11}O_2$, CAS# 307-24-4; 97% purity), Perfluoroheptanoic acid (PFHpA, $C_7HF_{13}O_2$, CAS#375-85-9; 99% purity) and Perfluorooctanoic acid (PFOA, $C_8HF_{15}O_2$, CAS#335-67-1; 96% purity) were purchased from sigma-Aldrich; Perfluorononanoic acid (PFNA, $C_9HF_{17}O_2$, CAS#375-95-1; 97% purity) was purchased from Shanghai Macklin Biochemical Co., Ltd; Perfluorodecanoic acid (PFDA, $C_{10}HF_{19}O_2$, CAS#335-76-2; 98% purity) was purchased from Shanghai Aladdin Biochemical Technology Co., Ltd.

Sodium chloride (0.01 M) was used as the background electrolyte solution for all surface-tension measurements and miscible-displacement experiments to match the experiments and modeling research conducted in prior PFAS studies. All of the solutions were prepared using boiled ultra-pure water to eliminate the influence of air in the solutions.

A natural quartz sand whose mean grain diameter is 0.35 mm was used for all of the miscible-displacement experiments. This sand has been used in our prior PFAS transport studies, and is employed for the present student to allow direct comparison of results. The sand has a low total organic carbon content (0.04%) and minimal metal-oxide and clay-mineral contents. Hence, the sand is anticipated to exhibit relatively low magnitudes of solid-phase adsorption. This is desirable for the present study to allow specific focus on the impact of air–water interfacial adsorption on retention and transport, thereby enhancing the opportunity to characterize and quantify this targeted process.

2.2. Surface tension measurements

Surface tensions were measured to characterize the surface activities for the different chain-length PFCAs, and to determine values for the air-water interfacial adsorption coefficients. A surface tension meter (QBZY-1, Shanghai Fangrui Instrument Co., Ltd., China) was used to measure the surface tension of aqueous C4-C10 PFCAs solutions at 1 mg/L (with 0.01 M NaCl). Full surface-tension curves for C4-C10 were also measured. Each sample was measured three times with a deviation between measurements of less than 0.1 mN/m.

The surface excess Γ (mol/cm^2) of a compound at the interface is related to the aqueous phase concentration (C) using the Gibbs adsorption equation (e.g., Fridrikhsberg, 1986; Hiemenz, 1986; Barnes and Gentle, 2005; Berg, 2010; Rosen and Kunjappu, 2012; Kronberg et al., 2014):

$$\Gamma = \frac{-1}{xR_gT}\frac{\partial\gamma}{\partial lnC} \tag{1}$$

where γ is the interfacial tension (dyn/cm or mN/m), C represents the aqueous phase concentration (mol/cm^3), T is temperature (K), R_g is the universal gas constant (dyne-cm/mol-K or J/mol-K), and x is a coefficient equal to 1 for systems with nonionic surfactants (or ionic surfactants with excess electrolyte in solution), and equal to 2 for systems with ionic surfactants without excess electrolyte (e.g., deionized water). The Gibbs equation has been shown in innumerable studies to provide accurate representation of surfactant behavior at fluid-fluid interfaces.

The air-water interfacial adsorption coefficient can be determined as:

$$K_{ia} = \frac{\Gamma}{C} = \frac{-1}{xR_gTC}\frac{\partial\gamma}{\partial lnC} \tag{2}$$

K_{ia} can be determined for any given aqueous concentration by calculating the local slope of surface tension versus ln C (i.e., $\partial\gamma/\partial$ ln C in

Eqs. (1) and (2)) through use of a tangent taken at the concentration of interest and dividing by the relevant C (Eq. (2)). The Szyszkowski equation was applied to the measured surface-tension data sets to support the determination of Γ values and provide a uniform means of data analysis. Numerous authors have demonstrated that the Szyszkowski equation provides accurate representation of surfactant surface-tension and interfacial-tension data including for PFAS. One form of the equation is given as (e.g., Adamson, 1990):

$$\gamma = \gamma_0 \left[1 - B ln \left(1 + \frac{C}{A} \right) \right] \tag{3}$$

where γ_0 is the interfacial tension at [PFAS] = 0 (e.g., the surface tension of water with no PFAS), and A and B are parameters related to properties of the specific compound and of the homologous series, respectively. The best-fit functions were used to obtain the slope factors required for Eq. (1) for all data sets.

2.3. Miscible-displacement experiments

The miscible-displacement experiments were conducted with each respective PFCA present alone in solution, rather than employing a multiple-component PFCA solution. This was done to eliminate potential co-solute interactions, allowing a direct focus on chain-length impacts on transport. The primary experiments were conducted employing an input concentration of 1 mg/L for each PFCA. This concentration was selected because it was desired that the input concentration be larger than the critical reference concentration (CRC) for at least one of the PFCAs employed to facilitate the investigation of nonlinear air-water interfacial adsorption. Inspection of Table 1 shows that this is true for PFNA and PFDA. A higher input concentration could have been used so that the CRC was larger for additional PFCA. However, it was also desired to employ an input concentration that was within the range of concentrations observed at field sites for the media relevant to the focus of this study, which in this case is soil and soil pore water. Reported soil concentrations range over many orders of magnitude depending upon numerous factors (Brusseau et al., 2020a). Pore-water concentrations ranging from several ug/L to 10's of mg/L have been reported for AFFF-application sites (Davis et al., 2021; Quinnan et al., 2021). Such high pore-water concentrations in source zones at aqueous film forming foam (AFFF) sites are consistent with reported soil concentrations that range up to the 10's to 100's of mg/kg (Brusseau et al., 2020a). Hence, the use of 1 mg/L input concentrations is consistent with data measured for primary source sites. Additional data are reported for PFOA with input concentrations lower and higher than 1 mg/L to further investigate AWIA behavior.

The columns used in this study were constructed of acrylic, and are 15 cm long with inner diameters of 1.6 cm. Flow distributors were placed on the top and at the bottom of the column in contact with the porous media to help promote uniform fluid distribution and to support the media. The columns were packed incrementally with air-dried media to promote uniform packing. Peristaltic pumps (BT100-02, Baoding Qili Precision Pump Co., Ltd., China) were used to provide fluid flow. Prior tests have indicated no measurable impact of PFAS sorption by the system.

The experiments were conducted using methods used in our previous studies (Lyu et al., 2018; Yan et al., 2020; Brusseau et al., 2021). Experiments were first conducted with individual solutions of C4-C10 PFCAs under saturated conditions to determine the impact of solid-phase sorption on retardation and transport. Experiments were then conducted under steady-state unsaturated conditions to determine the additional impact of air-water interfacial adsorption. Two pumps were connected to the column for the unsaturated-flow experiments. One was connected to the top to inject solution, and one to the bottom where solution was withdrawn at the same flow rate of 0.5 mL/min ($\Delta < 0.001$ mL/min) to maintain steady flow.

The unsaturated-flow experiments were conducted for a water saturation of approximately 0.7 (Table 1). The solution pH was 7 for all experiments. All experiments were conducted at room temperature (20 ± 1 °C). Prior reported data for GenX (Yan et al., 2020) and PFOS (Brusseau et al., 2021) are used for comparison purposes to investigate molecular-structure effects for AWIA.

Table 1
Transport experiments: conditions and results.

PFCA	Water saturation	F_{awia} [a]	CRC [b] (mg/L)
C4	0.68	0.04	700
C5	0.69	0.08	250
C6	0.68	0.18	100
C7	0.68	0.40	30
C8	0.68	0.63	10
C9	0.70	0.76	0.9
C10	0.70	0.74	0.4
GenX	0.62	0.68	30
PFOS	0.68	0.83	1

[a] Fraction of retention associated with adsorption at the air–water interface (see Eq. (5)).
[b] CRC is the critical reference concentration determined from the surface-tension data measured for 0.01 M NaCl solution.

2.4. Analytical methods

Methods used for analysis are similar to those used successfully in our prior research. The PFAS were analyzed by high-performance liquid chromatography (Thermo Model U3000, USA) and tandem mass spectrometry (TSQ quantum, Thermo Scientific, USA), i.e., LC-MS/MS. An Agilent C18 column (Hypersil GOLD VANQUIS, 1.9 um, 100 × 2.1 mm) was used, with the column temperature set and maintained at 50 °C. The dual mobile phase comprised 5 mM ammonium acetate and acetonitrile applied in a 60:40 gradient at a flow rate of 0.3 mL/min. Each column effluent sample was filtered by membrane and then injected directly, with injection volumes of 1 μL. The results of preliminary tests revealed the absence of any interferences associated with the membrane. Blanks and background aqueous samples collected from the column effluent before injection of PFAS revealed no measurable PFAS concentrations or other interferences for all experiments. The quantitative detection limits ranged from approximately 1 to 5 μg/L.

2.5. Data analysis

Measured retardation factors were determined for each miscible-displacement experiment by the standard methods of calculating the area above the breakthrough curve (frontal analysis) and temporal moment analysis. Tail extrapolation (e.g., Brusseau, 2021) was used in the moment analysis of the BTCs for PFNA and PFDA to account for the truncation of the elution fronts. The data-analysis methods have been demonstrated to be robust for PFAS applications (Brusseau et al., 2019a; Van Glubt et al., 2021). The retardation factors incorporate the contributions of all relevant retention processes influencing transport. The standard retardation factor (R) for aqueous phase transport of solute undergoing retention by adsorption to solid–water and air–water interfaces is given as (e.g., Lyu et al., 2018):

$$R = 1 + K_d \frac{\rho_b}{\theta_w} + K_{ia} \frac{A_{ia}}{\theta_w} \tag{4}$$

where K_d is the solid-phase adsorption coefficient (cm^3/g), A_{ia} is the specific air–water interfacial area (cm^2/cm^3), ρ_b is porous-medium bulk density (g/cm^3), and θ_w is volumetric water content (cm^3/cm^3). By phase balance, $\theta_w + \theta_a = n$, where θ_a is volumetric air content (cm^3/cm^3) and n is porosity. Water saturation is defined as $S_w = \theta_w/n$. The definition of R is revised for cases with nonlinear adsorption (Guo et al., 2020).

The fraction of the measured total retention associated with adsorption at the air–water interface is determined as:

$$F_{AWIA} = [(R - 1 - K_d \rho_b / \theta_w] / [R - 1] \tag{5}$$

Measured K_{ia} values are determined from the miscible-displacement experiments by rearranging Eq. (4), with R obtained from analysis of the breakthrough curve and all other variables determined independently: $K_{ia} = (\text{R-1-}K_d \frac{\rho_b}{\theta_w}) \frac{\theta_w}{A_{ia}}$. Values for A_{ia} for the sand have been measured in our prior studies (Brusseau et al., 2020b; Brusseau and Guo, 2021; El Ouni et al., 2021).

K_{ia} values are required for modeling and risk assessment of PFAS transport and fate. The QSPR analysis method can be used to provide empirical-based estimates when measured K_{ia} values for individual PFAS are not available. This approach is widely used to estimate phase-transfer (partition) coefficients, and proved to provide robust determination of K_{ia} values for different PFAS in recent studies (Lyu et al., 2018; Brusseau, 2019a; Brusseau and Van Glubt, 2019, 2021). QSPR analysis employs a wide variety of molecular descriptors. This study employs two simple ones, carbon number and molar volume (V_m). Details of the QSPR methods applied in this study are provided in our prior studies (Brusseau, 2019a; Brusseau and Van Glubt, 2019, 2021).

2.6. Mathematical modeling

A one-dimensional numerical model that couples transient, variably saturated flow and advective and dispersive transport is used to simulate PFAS transport (Guo et al., 2020). The model accounts for surfactant-induced flow, nonlinear, rate-limited solid-phase sorption, and nonlinear, rate-limited air-water interfacial adsorption. This model has been demonstrated to provide accurate simulations of PFAS and hydrocarbon-surfactant transport measured in unsaturated-flow miscible-displacement experiments (Brusseau et al., 2021; El Ouni et al., 2021; Zeng et al., 2021). The model is used in a predictive mode for simulation of PFAS transport in the unsaturated systems, with values for all input variables determined independently as described in Brusseau et al. (2021). Details of the model and its application are presented in Guo et al. (2020) and Brusseau et al. (2021), respectively.

Preliminary simulations were conducted to test the impact of surfactant-induced flow on transport under the conditions of the experiments. Two sets of simulations were conducted, one set with this process included and one set without. The results indicate no significant impact of surfactant-induced flow for the extant experiment conditions, which is as expected given that there are minimal to relatively small reductions in surface-tensions for the input concentration employed (see Fig. 1). These results are consistent with those of our prior transport experiments (Brusseau et al., 2021).

3. Results and discussion

3.1. Surface tensions

Surface tensions for 1 mg/L solutions of the C4-C10 PFCAs as a function of fluorinated carbon number and molar volume are presented in Fig. 1. The surface tensions decrease nonlinearly with the increase of carbon number and molar volume. The surface tensions of the PFCAs as a function of aqueous concentration exhibit different magnitudes of surface activities as a function of fluorinated carbon number (data not shown). This is consistent with prior studies (e.g., Lunkenheimer et al., 2015).

Surface tensions for surfactants with different surface activities can be compared by scaling the aqueous concentrations. A number of scaling approaches are available (Brusseau, 2021; Brusseau and Van Glubt, 2021). Brusseau (2021) presented a method wherein the aqueous concentrations are scaled in relation to the surface activity of a reference PFAS, such as PFOA. This is accomplished through application of a scaling factor, which can be determined for each PFAS based on comparison of the critical reference concentration of the individual PFAS to that of the selected reference PFAS (PFOA in this case). The CRC is defined as the inflection point in the surface/interfacial-tension curve (Brusseau, 2019a; Brusseau and Van Glubt, 2021). This scaling factor represents the relative surface-activity strength of a given surfactant compared to that of PFOA. This approach allows the use of actual concentration units rather than normalized units. The surface-tension functions scaled in this manner are presented in Fig. 2. Notably, the scaled surface tensions of all PFCAs are congruent and can be represented with a single Szyszkowski function, indicating similar surface-activity behavior.

The potential nonlinearity of air-water interfacial adsorption can be assessed by comparing the input concentration of 1 mg/L used for the transport experiments to the respective CRC for each PFCA. The CRC represents the concentration below which there is minimal change in surface tension (Brusseau, 2019a; Brusseau, 2021; Brusseau and Van Glubt, 2021). As a result, K_{ia} values calculated from surface-tension data attain an essentially constant, maximum value below this concentration. The CRC can be determined from the inflection point of the surface-tension function. For this study, the concentration at which the surface tension decreased by ~2.5% was used to calculate the values (Brusseau and Van Glubt, 2021), which are reported in Table 1. Log CRC is a linear function of molar volume, reflecting the influence of molecular size on surface activity (Brusseau and Van Glubt, 2021).

The 1 mg/L input concentration is more than one or two orders-of-magnitude below the CRCs for the shorter-chain PFCAs (Table 1). Hence, K_{ia} values determined from surface-tension data will be essentially constant and air-water interfacial adsorption is anticipated to be essentially linear for the transport of these PFCAs. Conversely, the CRC is lower than the input concentration for the two longest-chain PFCAs. Thus, the transport of the longest-chain PFCAs is expected to be influenced by nonlinear air-water interfacial adsorption to some extent as K_{ia} will vary within the concentration range of the transport experiments. The nonlinearity of air-water interfacial adsorption under transport conditions will be examined in forthcoming sections.

3.2. PFCA retention and transport

Effluent recoveries for the saturated- and unsaturated-flow experiments averaged 99.5 (±3%) and 97.3 (±2%), respectively, indicating essentially

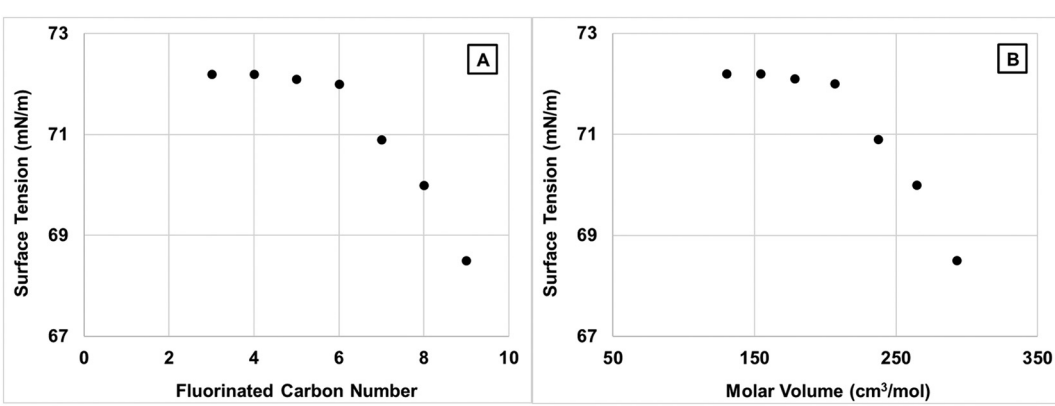

Fig. 1. Surface tensions of 1 mg/L PFCA solutions as a function of (A) PFAS fluorinated carbon number and (B) molar volume.

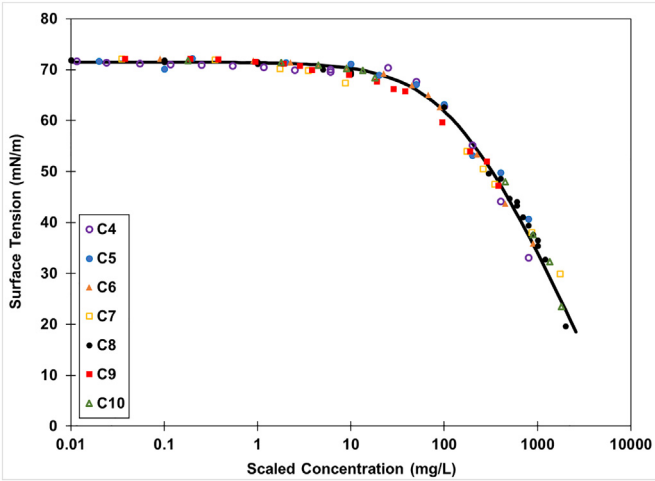

Fig. 2. Surface tensions as a function of PFCA concentration, with the aqueous concentrations scaled to the surface activity of PFOA (as described in the text). Scaling factors: C4- 0.01, C5- 0.02, C6- 0.09, C7- 0.35, C8- 1, C9- 3.8, and C10- 18.

complete recovery within analytical uncertainty. The breakthrough curves (BTCs) for transport of the PFCAs under unsaturated conditions exhibit greater retardation compared to saturated conditions, especially for the longer-chain PFCAs. This is illustrated in Fig. 3. This greater retardation reflects the impact of the additional retention associated with adsorption at the air–water interface that occurs under unsaturated conditions. Significantly greater retardation is observed for the long-chain PFCAs compared to the short-chain PFCAs.

The fraction of total retention associated with air–water interfacial adsorption (F_{awia}) can be determined by subtracting the contribution of solid-phase sorption from the total measured retention (Eq. (5)). Air–water interfacial adsorption contributes 4%–40% of the overall retention for the short-chain PFCAs (Table 1). Hence, solid-phase sorption provides the majority of retention for the C4-C7 PFCAs, with air-water interfacial adsorption providing a lesser contribution. Conversely, air-water interfacial adsorption provides the majority (>60%) of total retention for the C8-C10 PFCAs. This disparity in the significance of air-water interfacial adsorption reflects the significantly greater surface activities of the long-chain PFCAs, as previously discussed with respect to the surface-tension data.

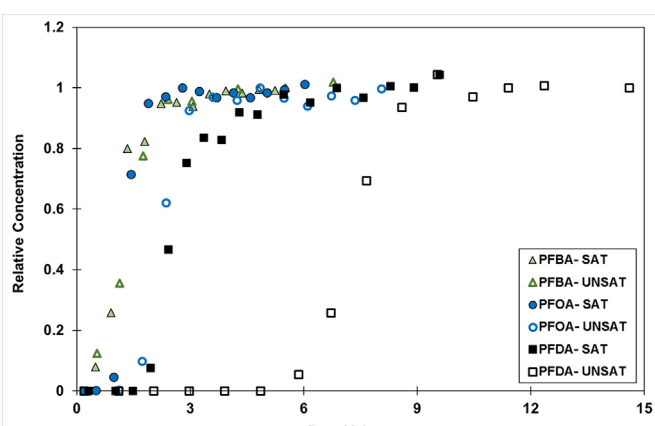

Fig. 3. Measured breakthrough curves for transport of PFBA, PFOA, and PFDA under saturated and unsaturated-flow conditions. Relative concentration represents the measured concentration in the effluent sample divided by the input concentration. Pore volumes represent the volumetric discharge divided by the resident water volume within the packed column. Only the arrival fronts are presented to enhance visualization of the differences in retardation. Water saturations for the unsaturated-flow experiments are reported in Table 1.

The relative significance of air-water interfacial adsorption versus solid-phase sorption will also depend upon the properties and conditions of the porous medium, in addition to those of the PFAS. First, the sorption capacity of the porous medium is a function of the geochemical composition of the solid and solution phases. Second, porous-medium properties mediate the magnitude of air-water interfacial area associated with the medium. Third, the magnitude of air-water interfacial area is a function of water saturation. The influence of porous-medium properties is illustrated by the results of Brusseau et al. (2019a), who reported that air-water interfacial adsorption contributed 83% of the total retention for PFOS transport in the sand used for the current study versus 32% for transport in a soil that has greater sorption capacity compared to the sand.

The relative significance of the retention processes can influence the measurement uncertainty. For example, measurement uncertainty is likely to be greater for conditions wherein the relative magnitude of a particular retention process is comparatively small. However, the practical impact of this greater measurement uncertainty is limited by the fact that the overall contribution of that retention process to transport is comparatively minimal.

3.3. PFCA transport behavior

To fully understand transport behavior it is of interest to evaluate if the relevant adsorption processes are rate limited or nonlinear under the extant experiment conditions. One standard evaluation approach comprises the examination of BTC profiles as a function of changes in solutes or experimental conditions. Such comparisons are facilitated by normalizing the pore volumes of each BTC by the respective retardation factor of each solute (Brusseau et al., 1991; Russo et al., 2010). Representative normalized BTCs are presented in Fig. 4 for PFHxA and PFDA. It is observed that the BTC for PFDA transport under unsaturated conditions is skewed, exhibiting a sharp arrival front and an elution front with extended concentration tailing. Similar behavior is observed for the transport of PFNA (data not shown). Conversely, the PFDA BTC for saturated conditions exhibits a distinctly different profile, with extended tailing present for both the arrival and elution fronts. The presence of extended tailing for both fronts is a common characteristic of the impact of rate-limited mass transfer on transport. The results of mathematical modeling indicate that the nonideal transport observed for the saturated-flow BTCs is caused primarily by rate-limited sorption, with a minor contribution from nonlinear sorption. This is consistent with prior results reported for PFOA and PFOS transport in sand, aquifer media, and soils (Brusseau et al., 2019b; Wang et al., 2021). In contrast to the disparate behavior observed for PFDA, the BTCs for the short-chain PFCAs exhibit similar profiles for both saturated and unsaturated conditions (see Fig. 4). Their BTCs are not skewed for unsaturated conditions, and they exhibit a small degree of tailing for both fronts.

The preceding results indicate that the transport of PFNA and PFDA under unsaturated conditions is influenced by nonlinear air-water interfacial adsorption, whereas the transport of the shorter-chain PFCAs is not. Hence, the effective K_{ia} varies to some degree during transport for PFNA and PFDA, whereas it is essentially constant for the shorter-chain PFCAs. These results are consistent with the discussion presented in Section 3.1 concerning the comparisons of the input concentration used for the transport experiments versus the CRCs determined from the surface-tension data. As noted, the input concentration of 1 mg/L is much lower than the respective CRCs for all of the PFCA except PFNA and PFDA. The present results for the shorter-chain PFCAs are consistent with those of prior experiments conducted for PFOA transport in the same sand, which demonstrated that air-water interfacial adsorption was linear for experiments conducted with input concentrations approximately 10-times lower than the CRC (Brusseau et al., 2021).

Nonideal transport behavior can be further assessed by examining retardation-normalized elution-front profiles on a semi-log scale to evaluate lower-concentration elution behavior (Russo et al., 2010). Such an approach was used for example to investigate nonideal transport and extended elution tailing of PFOS in saturated soils (Brusseau et al. 2019b)

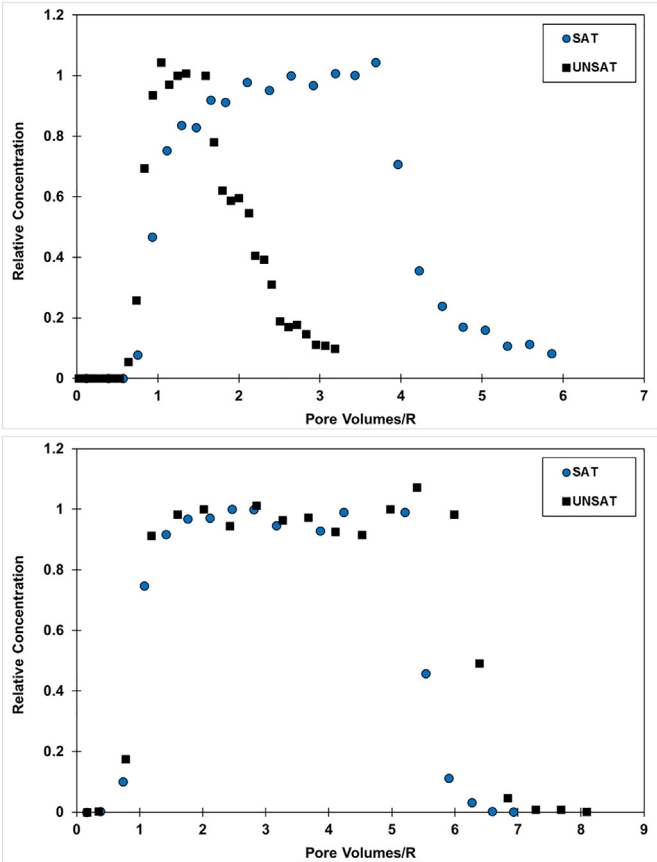

Fig. 4. Measured breakthrough curves for transport of (top) PFDA and (bottom) PFHxA under saturated and unsaturated-flow conditions. Relative concentration represents the measured concentration in the effluent sample divided by the input concentration. Pore volumes represent the volumetric discharge divided by the resident water volume within the packed column. The pore volumes are normalized by the respective retardation factor of the PFCA. Water saturations for the unsaturated-flow experiments are reported in Table 1.

and aquifer sediments (Wang et al., 2021). Normalized data sets are presented in Fig. 5 for three PFAS. Inspection of Fig. 5 shows that the normalized elution fronts for PFHxA and GenX are essentially identical for saturated and unsaturated conditions. Significant impacts of either rate-limited or nonlinear air-water interfacial adsorption on transport would lead to elution fronts that exhibit greater tailing for unsaturated conditions compared to saturated conditions. Hence, the congruent elution fronts indicate that air-water interfacial adsorption is effectively instantaneous and linear for transport of both PFAS. This is consistent with the results of prior analyses of PFAS transport data (Brusseau, 2020; Brusseau et al., 2021). Notably, this is observed for both PFHxA and GenX, for which the relative contributions of air-water interfacial adsorption to total retention are significantly different (Table 1).

In contrast to PFHxA and GenX, the PFNA elution fronts for transport under unsaturated conditions exhibit significantly greater tailing compared to those for saturated conditions. This indicates that air-water interfacial adsorption is either nonlinear or rate-limited for PFNA transport. Rate-limited adsorption processes typically produce extended concentration tailing for both the arrival front and the elution front, as illustrated in Fig. 4 for the saturated-flow BTCs. The PFNA and PFDA BTCs for unsaturated-flow conditions do not exhibit significant arrival-front tailing, as discussed above. In addition, as previously noted, the BTCs for PFNA and PFDA exhibit the classic skewed profiles associated with nonlinear adsorption. Therefore, the disparity in saturated- vs unsaturated-flow elution-front profiles for PFNA is attributed to the impact of nonlinear air-water interfacial adsorption.

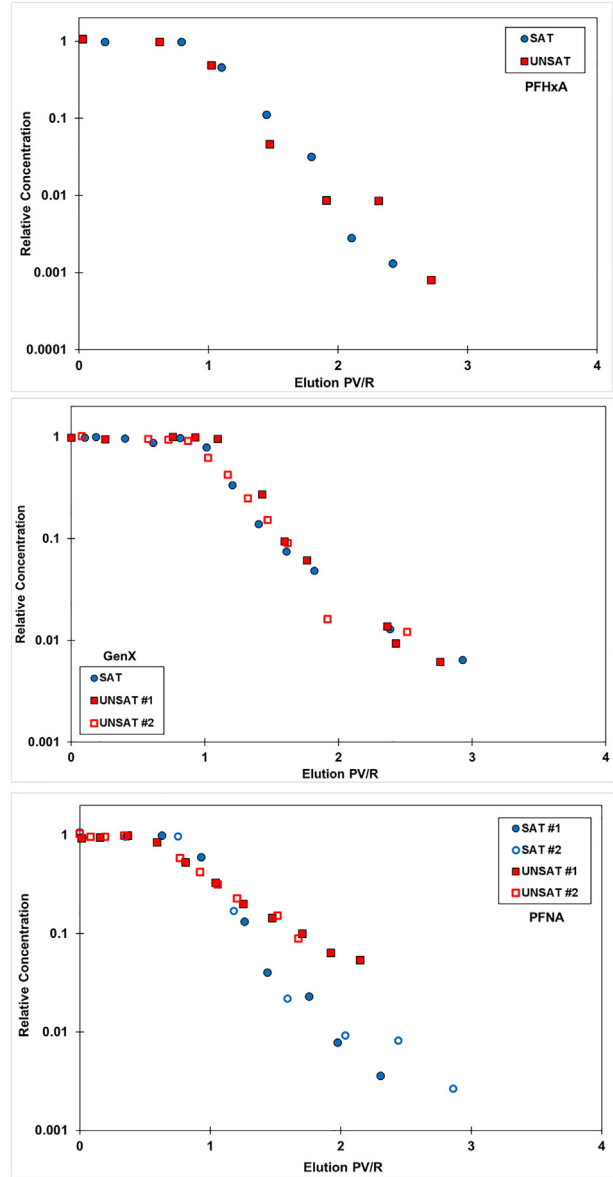

Fig. 5. Normalized elution fronts for PFHxA (top), GenX (middle), PFNA (bottom) for transport under saturated and unsaturated conditions. The elution-front eluted pore volumes are normalized by the respective retardation factor of each PFCA. Input concentrations are 1, 0.01, and 1 mg/L for PFHxA, GenX, and PFNA, respectively. GenX data are from Yan et al. (2020). The appellations #1 and #2 represent duplicate experiments.

To further test the non-linearity of air-water interfacial adsorption, two sets of PFCA transport simulations were conducted. One set with AWIA treated as nonlinear (K_{ia} is a function of concentration) and the other with AWIA treated as linear, wherein the maximum surface-tension measured K_{ia} values were used for the latter simulations. The simulations for linear and nonlinear air-water interfacial adsorption are essentially identical for the C4-C8 PFCAs, indicating minimal impact of nonlinear AWIA on the transport of these PFCAs under the extant conditions. Conversely, nonlinear air-water interfacial adsorption was shown to influence the transport of C9 and C10. A comparison of normalized elution fronts for unsaturated flow is presented in Fig. 6 for C5, C6, C9, and C10. Also included is the independently-predicted normalized simulation for which AWIA is treated as linear and instantaneous. The measured elution fronts for C9 and C10 exhibit significantly greater tailing compared to those for C5 and C6. In addition, the predicted simulation provides a good representation of the measured elution fronts for C5 and C6, but not for C9 and C10.

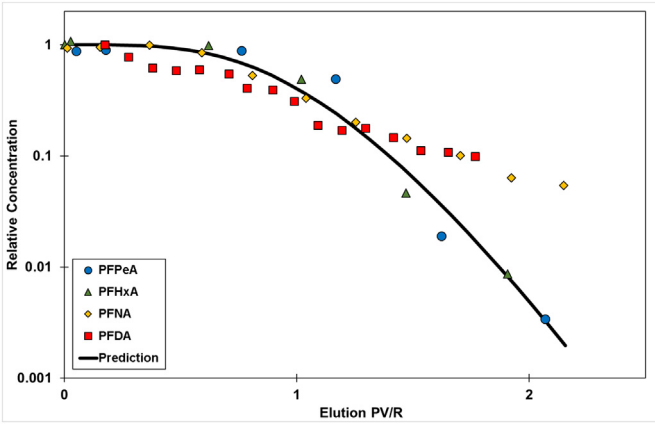

Fig. 6. Normalized elution fronts for PFPeA, PFHxA, PFNA, and PFDA for transport under unsaturated conditions. The elution-front eluted pore volumes are normalized by the respective retardation factor of each PFCA. Input concentration is 1 mg/L. The solid curve represents a predicted simulation representing transport with instantaneous and linear air-water interfacial adsorption.

The analyses presented with Figs. 5 and 6 comprise comparisons of different PFAS that have different CRCs. Another means by which to assess the nonlinearity of air-water interfacial adsorption is to compare normalized elution fronts for experiments conducted with different input concentrations for the same PFAS. Such a comparison is presented in Fig. 7 for PFOA and PFOS. Also presented are the independently-predicted simulations for which air-water interfacial adsorption is treated as linear and instantaneous. The elution fronts measured for the lower input-concentration experiments exhibit tailing that is fully consistent with the predicted simulations for both PFOA and PFOS. This indicates that air-water interfacial adsorption is effectively linear and instantaneous for transport at these lower input concentrations. Notably, the input concentrations for these cases are significantly below the respective CRCs of PFOA and PFOS (Table 1). In contrast, the elution fronts for the experiments conducted with input concentrations near or above the CRCs exhibit enhanced tailing that deviates from the predicted simulations. This enhanced tailing is consistent with that observed in Fig. 6 for PFNA and PFDA. The additional tailing is attributed at least in part to the impact of nonlinear air-water interfacial adsorption as discussed above.

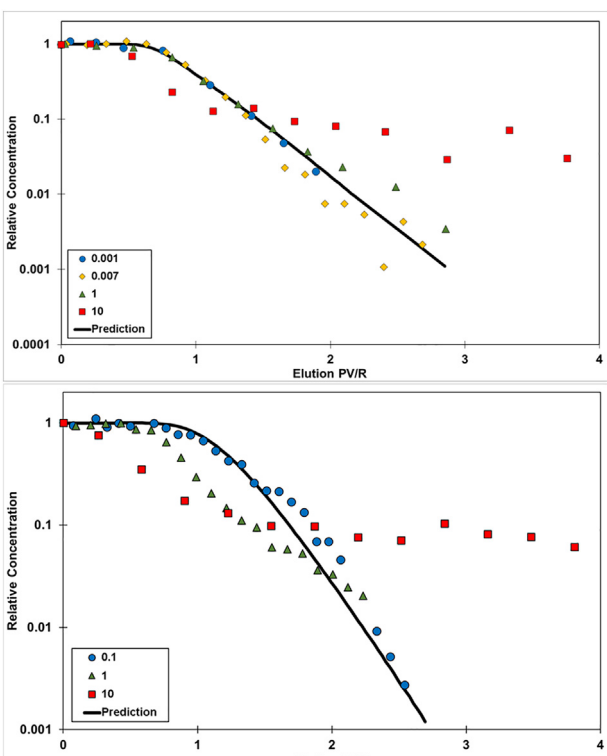

Fig. 7. Normalized elution fronts for PFOA (top) and PFOS (bottom) for transport under unsaturated conditions. The elution-front eluted pore volumes are normalized by the respective retardation factor of each PFCA. The input concentrations reported in the legends are in units of mg/L. The solid curve represents a predicted simulation representing transport with instantaneous and linear air-water interfacial adsorption. The PFOA 0.001 and 10 data and all PFOS data are from Brusseau et al. (2021); the PFOA 0.007 data are from Li et al. (2021).

3.4. Air-water interfacial adsorption coefficients

Air-water interfacial adsorption coefficients were determined from the unsaturated-flow transport experiments as described in Section 2.5. The K_{ia} value for PFOA is 0.00285 cm for the 1 mg/L input concentration used for the transport experiments. Brusseau et al. (2021) compiled K_{ia} values for PFOA measured from prior transport experiments and determined a mean value of 0.00285 cm from 7 separate experiments for a concentration of 1 mg/L. The K_{ia} value measured in the present study is identical to the mean of the prior experiments, indicating excellent consistency of the experimental methods.

A comparison of air-water interfacial adsorption coefficients determined from the transport experiments to those determined from the surface-tension data is presented in Fig. 8. The two sets of values are observed to be similar, which has multiple implications. First, it indicates that air-water interfacial adsorption kinetics were minimal during transport, given that the K_{ia} values determined from surface-tension measurements represent equilibrium values. Second, it indicates that the miscible-displacement experiments produced consistent and robust measurements of air-water interfacial adsorption. Third, it indicates that surface-tension measurements can be used to determine K_{ia} values that are representative for transport conditions. This is consistent with the results obtained from our prior studies (Lyu et al., 2018; Brusseau et al., 2019b; Yan et al., 2020; Brusseau, 2021; Brusseau et al., 2021).

An excellent linear relationship between log K_{ia} and fluorinated carbon number exists for all PFCAs (Fig. 9). Log K_{ia} is observed to increase ~0.46 for each increase in fluorinated carbon in the chain. This is similar to values reported in prior studies for air-water interfacial adsorption (Brusseau, 2019b) and solid-phase sorption (Higgins and Luthy, 2006; Guelfo and Higgins, 2013; Milinovic et al., 2015; Brusseau, 2019b). The linear log K_{ia} − carbon-number relationship translates to a nonlinear relationship between R and carbon number (Fig. 9). The plot shows that air-water

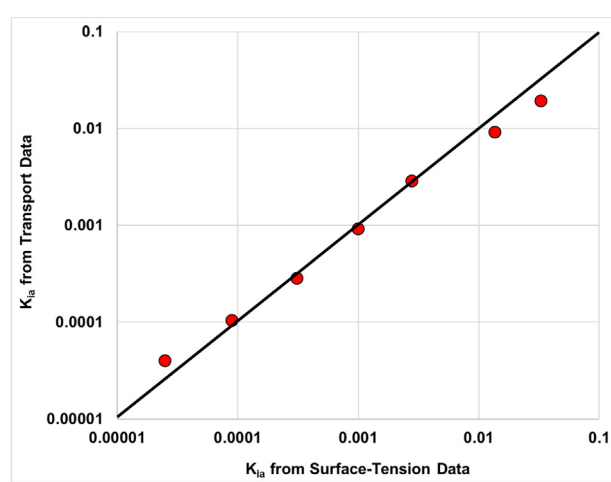

Fig. 8. Comparison of air-water interfacial adsorption coefficients (K_{ia}, cm) determined from the transport experiments versus from surface-tension data. The solid line represents the one-to-one correlation.

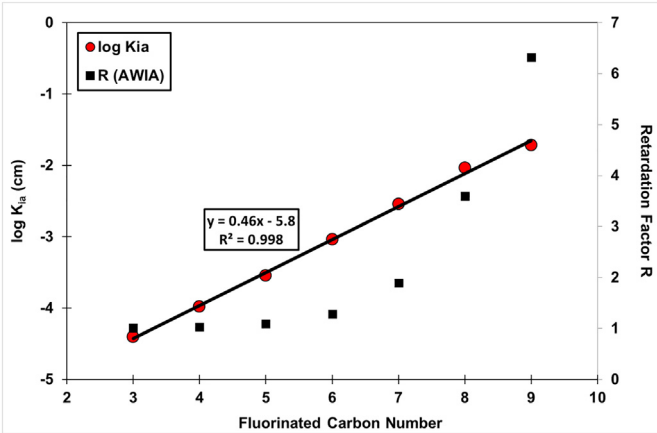

Fig. 9. Correlation of air–water interfacial adsorption coefficient (K_{ai}) and retardation factor R (accounting solely for air–water interfacial adsorption) determined from transport experiments versus fluorinated carbon number for C4-C10 PFCAs. K_{ai} values are measured for [PFCA] = 1 mg/L.

interfacial adsorption does not contribute significantly for the short-chain PFCAs, consistent with the F_{AWIA} values. Both the log K_{ia} and R relationships presented in Fig. 9, which are based on transport-measured data, are consistent with the log K_{ia} and R relationships reported by Lyu et al. (2018) that were based on surface-tension measurements.

The QSPR model employing molar volume (V_m) as a descriptor also provides robust characterization of the log K_{ia} values (Fig. 10). Notably, previously reported transport-measured values for GenX and PFOS are consistent with the C4-C10 values. These results are also consistent with our prior QSPR analyses of K_{ia} values based on surface-tension data (Brusseau, 2019a; Brusseau and Van Glubt, 2019, 2021). As discussed in those prior works, the molar volume descriptor provides a representation of the influence of molecular size on cavity formation and destruction in solution (hydrophobic interactions) which is the driving force for interfacial adsorption of surfactants. The QSPR analyses presented in Figs. 9 and 10 represent the first such relationships developed using transport-measured K_{ia} values. Comparison of Figs. 9 and 10 shows that both molar volume and carbon number serve as robust molecular descriptors for this homologous series of PFCAs. However, molar volume was demonstrated to be the more robust descriptor for a broader range of PFAS molecular structures (Brusseau, 2019a).

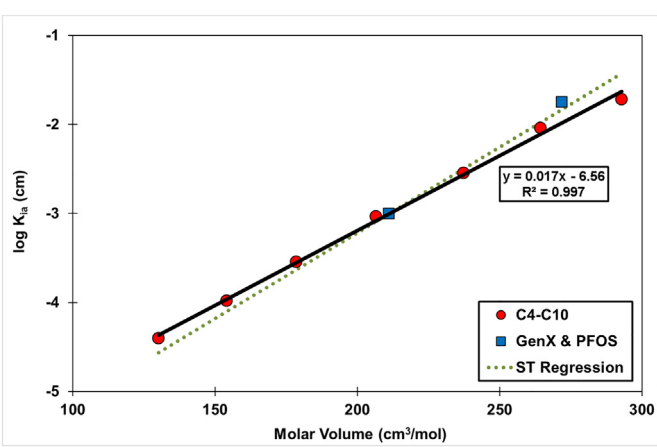

Fig. 10. QSPR analysis of log K_{ia} measured from transport experiments for C4-C10 PFCAs. Also shown are transport-measured values for GenX (left point) and PFOS (right point) reported in our prior studies (Brusseau et al., 2019a; Yan et al., 2020). The "ST-Regression" curve represents the regression obtained for K_{ia} determined from surface-tension data measured for PFAS in electrolyte solution (Brusseau and Van Glubt, 2021).

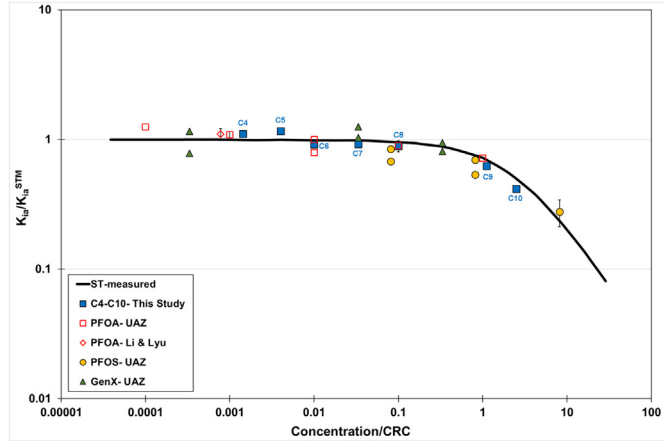

Fig. 11. Comparison of air-water interfacial adsorption coefficients (K_{ia}) measured from transport experiments (represented by various symbols) and surface-tension data (ST-measured, solid curve) as a function of solution concentration. The measured values are scaled by the respective maximum surface-tension K_{ia} value ($K_{ia}^{S\,TM}$) of each PFAS. The solution concentrations are scaled by the respective critical reference concentrations (CRC) to facilitate direct comparison of the different PFAS. The PFOA-UAZ, PFOS-UAZ, and GenX-UAZ data are from Brusseau et al. (2019a), Yan et al. (2020). The Li & Lyu data are from Li et al. (2021) and Lyu et al. (2020).

As discussed in Section 3.1, K_{ia} values determined from surface-tension data are a function of concentration at higher ranges of concentration, and approach a maximum value at lower concentrations. This behavior is illustrated in Fig. 11, wherein the solid curve represents the K_{ia} value determined from surface-tension data at a given solution concentration scaled by the maximum surface-tension K_{ia} value ($K_{ia}^{S\,TM}$). Brusseau et al. (2021) compared K_{ia} values measured from transport data for PFOA, PFOS, and GenX to surface-tension based values as a function of solution concentration. A similar comparison is presented in Fig. 11, where these transport-measured values are scaled by the respective $K_{ia}^{S\,TM}$ of each PFAS. The solution concentrations are scaled by the CRC to facilitate direct comparison of the different PFAS. It is observed that the transport-based K_{ia} values measured for concentrations similar to or greater than the CRC are smaller than the maximum ($K_{ia}/K_{ia}^{S\,TM} < 1$), whereas those measured at concentrations below the CRC match the $K_{ia}^{S\,TM}$. The transport data measured in the present study can also be evaluated in this manner. Inspection of Fig. 11 shows that the C4-C10 K_{ia} data exhibit a concentration dependency consistent with that of the other data sets. Specifically, the $K_{ia}/K_{ia}^{S\,TM}$ for C9 and C10 are significantly <1, which is due to the impact of nonlinear adsorption as discussed previously. Conversely, the $K_{ia}/K_{ia}^{S\,TM}$ are unity for the shortest-chain PFCAs. These results support the prior discussions of linear versus nonlinear air-water interfacial adsorption.

4. Conclusions

This study represents the first direct experiment-based investigation of chain-length effects for air-water interfacial adsorption and retention of PFAS during transport in unsaturated porous media. The results of this study demonstrate that the magnitude of air–water interfacial adsorption under transport conditions correlates to PFAS chain length. The relative contributions of solid-phase sorption and air-water interfacial adsorption to total retention is also a function of chain length, with the latter the predominant contributor to retention for the long-chain PFCAs. Conversely, the contribution of solid-phase sorption was predominant for the short-chain PFCAs. The relative significance of AWIA versus solid-phase sorption will also depend upon the properties of the porous medium, which will mediate the sorption capacity and the magnitude of air-water interfacial area associated with the medium. QSPR analysis showed that log K_{ia} values were a linear function of fluorinated carbon number and molar volume. Air-water interfacial adsorption coefficients determined from the transport

experiments were consistent with those measured from surface-tension data, indicating that the transport experiments produced robust measurements of air-water interfacial adsorption.

The nonlinearity of air-water interfacial adsorption during transport was demonstrated to be a function of chain length for the input concentration employed in the experiments. Analysis of the measured and simulated transport data along with the surface-tension measurements indicates that air-water interfacial adsorption can be treated as linear when the concentration range of interest for transport is sufficiently below the CRC associated with surface activity. This allows simplification of mathematical modeling with the use of a constant K_{ia}.

Overall, the results of the study indicate that short-chain PFCAs will experience relatively less air-water interfacial adsorption and associated retention during transport in unsaturated porous media compared to longer-chain PFCAs. This has significant implications for assessing migration and leaching potential of PFAS in soil and the vadose zone. Additional research is needed to investigate the transport of PFAS mixtures under unsaturated conditions.

CRediT authorship contribution statement

Ying Lyu: Conceptualization, Resources, Methodology, Investigation, Analysis, Writing- Original draft preparation.

Baohua Wang: Investigation, Writing- Review & Editing.

Xinqiang Du: Investigation, Writing- Review & Editing.

Bo Guo: Investigation, Analysis, Writing- Review & Editing.

Mark L. Brusseau: Conceptualization, Resources, Methodology, Investigation, Analysis, Writing- Review & Editing, Supervision.

Declaration of competing interest

The authors declare that they have no known competing financial interests or personal relationships that could have appeared to influence the work reported in this paper.

Acknowledgements

This work was supported by the National Natural Science Foundation of China (#41902247), the Thirteenth Five-Year Science and Technology Project of Jilin Province Education Department (JJKH20201005KJ), the NIEHS Superfund Research Program (grant #P42 ES04940), and the National Science Foundation Hydrologic Sciences Program (#2023351). We thank the reviewers for their constructive comments.

References

Adamson, A.W., 1990. Physical Chemistry of Surfaces. 5th ed. Wiley.

Ahrens, L., 2011. Polyfluoroalkyl compounds in the aquatic environment: a review of their occurrence and fate. J. Environ. Monit. 13 (1), 20–31.

Allred, B., Brown, G.O., 1996. Anionic surfactant transport characteristics in unsaturated soil. Soil Sci. 161, 415–425.

Allred, B., Brown, G.O., 2001. Anionic surfactant mobility in unsaturated soil: the impact of molecular structure. Environ. Geosci. 8, 95–109.

Anderson, R.H., Long, G.C., Porter, R.C., Anderson, J.K., 2016. Occurrence of select perfluoroalkyl substances at U.S. Air Force aqueous film-forming foam release sites other than fire-training areas: field-validation of critical fate and transport properties. Chemosphere 150, 678–685.

Backe, W.J., Day, T.C., Field, J.A., 2013. Zwitterionic, cationic, and anionic fluorinated chemicals in aqueous film forming foam formulations and groundwater from U.S. Military bases by nonaqueous large-volume injection HPLC-MS/MS. Environ. Sci. Technol. 47 (10), 5226–5234.

Barnes, G., Gentle, I., 2005. Interfacial science: An introduction. Oxford University Press, New York, NY.

Berg, J.C., 2010. An Introduction to Interfaces & Colloids: the Bridge to Nanoscience. World Scientific Publishing Co, Singapore.

Brusseau, M.L., 2018. Assessing the potential contributions of additional retention processes to PFAS retardation in the subsurface. Sci. Total Environ. 613–614, 176–185.

Brusseau, M.L., 2019a. The influence of molecular structure on the adsorption of PFAS to fluid-fluid interfaces: using QSPR to predict interfacial adsorption coefficients. Water Res. 152, 148–158.

Brusseau, M.L., 2019b. Estimating the relative magnitudes of adsorption to solid-water and air/oil-water interfaces for per- and poly-fluoroalkyl substances. Environ. Pollut. 254, 113102.

Brusseau, M.L., 2020. Simulating PFAS transport influenced by rate-limited multi-process retention. Water Res. 168, 115179.

Brusseau, M.L., 2021. Examining the robustness and concentration dependency of PFAS air-water and NAPL-water interfacial adsorption coefficients. Water Res. 190, 116778.

Brusseau, M.L., Guo, B., 2021. Air-water interfacial areas relevant for transport of per and poly-fluoroalkyl substances. Water Res. 207, 117785.

Brusseau, M.L., Van Glubt, S., 2019. The influence of surfactant and solution composition on PFAS adsorption at fluid-fluid interfaces. Water Res. 161, 17–26.

Brusseau, M.L., Van Glubt, S., 2021. The influence of molecular structure on PFAS adsorption at air-water interfaces in electrolyte solutions. Chemosphere 281, 130829.

Brusseau, M.L., Jessup, R.E., Rao, P.S.C., 1991. Nonequilibrium sorption of organic chemicals: elucidation of rate-limiting processes. Environ. Sci. Technol. 25, 134–142.

Brusseau, M.L., Yan, N., Van Glubt, S., Wang, Y., Chen, W., Lyu, Y., Dungan, B., Carroll, K.C., Holguin, F.O., 2019a. Comprehensive retention model for PFAS transport in subsurface systems. Water Res. 148, 41–50.

Brusseau, M.L., Khan, N., Wang, Y.K., Yan, N., Van Glubt, S., Carroll, K.C., 2019b. Nonideal transport and extended elution tailing of PFOS in soil. Environ. Sci. Technol. 53, 10654–10664.

Brusseau, M.L., Anderson, R.H., Guo, B., 2020a. PFAS concentrations in soils: Background levels versus contaminated sites. Sci. Total Environ. 740 article 140017.

Brusseau, M.L., Lyu, Y., Yan, N., Guo, B., 2020b. Low-concentration tracer tests to measure air-water interfacial area in porous media. Chemosphere 250, 126305.

Brusseau, M.L., Guo, B., Huang, D., Yan, N., Lyu, Y., 2021. Ideal versus nonideal transport of PFAS in unsaturated porous media. Water Res. 202, 117405.

Buck, R.C., Franklin, J., Berger, U., Conder, J.M., Cousins, I.T., de Voogt, P., Jensen, A.A., Kannan, K., Mabury, S.A., van Leeuwen, S.P., 2011. Perfluoroalkyl and polyfluoroalkyl substances in the environment: terminology, classification, and origins. Integr. Environ. Assess. Manag. 7 (4), 513–541. https://doi.org/10.1002/ieam.258.

Campos Pereira, H., Ullberg, M., Kleja, D.B., Gustafsson, J.P., Ahrens, L., 2018. Sorption of perfluoroalkyl substances (PFASs) to an organic soil horizon – Effect of cation composition and pH. Chemos. 207, 183–191.

Cousins, I.T., Vestergren, R., Wang, Z., Scheringer, M., McLachlan, M.S., 2016. The precautionary principle and chemicals management: the example of perfluoroalkyl acids in groundwater. Environ. Int. 94, 331–340.

Davis, G.B., Wallis, I., Kookana, R., Navarro, D., Rayner, J.L., Prommer, H., 2021. Key unsaturated zone soil processes for PFAS mobility and retention: principles and understanding. CSIRO, Australia Report for the PFAS Investigation & Management Branch, Department of 153 Defence.

El Ouni, A., Guo, B., Zhong, H., Brusseau, M.L., 2021. Testing the validity of the miscible-displacement interfacial tracer method for measuring air–water interfacial area: independent benchmarking and mathematical modeling. Chemosphere 263, 128193.

Fridrikhsberg, D.A., 1986. A Course on Colloid Chemistry. Mir Publishers, Moscow.

Guelfo, J.L., Higgins, C.P., 2013. Subsurface transport potential of perfluoroalkyl acids at aqueous film-forming foam (AFFF)-impacted sites. Environ. Sci. Technol. 47 (9), 4164–4171.

Guo, B., Zeng, J., Brusseau, M.L., 2020. A mathematical model for the release, transport, and retention of per- and polyfluoroalkyl substances (PFAS) in the vadose Zone. Water Resour. Res. 56 (2), 21.

Hatton, J., Holton, C., DiGuiseppi, B., 2018. Occurrence and behavior of per- and polyfluoroalkyl substances from aqueous film-forming foam in groundwater systems. Remediation 28, 89–99.

Hiemenz, P.C., 1986. Principles of Colloid and Surface Chemistry. Second ed. Marcel Dekker: Inc, New York.

Higgins, C.P., Luthy, R.G., 2006. Sorption of perfluorinated surfactants on sediments. Environ. Sci. Technol. 40 (23), 7251–7256.

Krafft, M.P., Riess, J.G., 2015. Per- and polyfluorinated substances (PFASs): Environmental challenges. Curr. Opin. Colloid In. 20 (3), 192–212.

Kronberg, B., Holmberg, K., Lindman, B., 2014. Surface Chemistry of Surfactants and Polymers. West Sussex, England, John Wiley and Sons Ltd.

Li, Z., Lyu, X., Gao, B., Xu, H., Wu, J., Sun, Y., 2021. Effects of ionic strength and cation type on the transport of perfluorooctanoic acid (PFOA) in unsaturated sand porous media. J. Hazard. Mater. 403, 123688.

Lunkenheimer, K., Prescher, D., Hirte, R., Geggel, K., 2015. Adsorption properties of surface chemically pure sodium perfluoro-n-alkanoates at the air/water interface: counterion effects within homologous series of 1:1 ionic surfactants. Langmuir 31 (3), 970–981.

Lyu, Y., Brusseau, M.L., 2020. The influence of solution chemistry on air-water interfacial adsorption and transport of PFOA in unsaturated porous media. Sci. Total Environ. 713, 136744.

Lyu, Y., Brusseau, M.L., Chen, W., Yan, N., Fu, X., Lin, X., 2018. Adsorption of PFOA at the air-water interface during transport in unsaturated porous media. Environ. Sci. Technol. 52 (14), 7745–7753.

Lyu, X., Liu, X., Sun, Y., Gao, B., Ji, R., Wu, J., Xue, Y., 2020. Importance of surface roughness on perfluorooctanoic acid (PFOA) transport in unsaturated porous media. Envrion. Pollut. 266, 115343.

Milinovic, J., Lacorte, S., Vidal, M., Rigol, A., 2015. Sorption behaviour of perfluoroalkyl substances in soils. Sci. Total Environ. 511, 63–71.

Miller, W.W., Letey, J., 1975. Distribution of nonionic surfactant in soil columns following application and leaching. Proc. Soil Sci. Soc. Am. 39, 17–22.

Mingorance, M.D., Fernaandez Gaalvez, J., Pena, A., Barahona, E., 2007. Laboratory methodology to approach soil water transport in the presence of surfactants. Colloids SurfA 306, 75–82.

Nguyen, T.M.H., Braunig, J., Thompson, K., Thompson, J., Kabiri, S., Navarro, D.A., Kookana, R.S., Grimison, C., Barnes, C.M., Higgins, C.P., McLaughlin, M.J., Mueller, J.F., 2020. Influences of chemical properties, soil properties, and solution pH on soil-water partitioning coefficients of per- and polyfluoroalkyl substances (PFASs). Environ. Sci. Technol. 54 (24), 15883–15892.

Quinnan, J., Rossi, M., Curry, P., Lupo, M., Miller, M., Korb, H., Orth, C., Hasbrouck, K., 2021. Application of PFAS-mobile lab to support adaptive characterization and flux-based conceptual site models at AFFF releases. Remediation 31, 7–26.

Rankin, K., Mabury, S., Jenkins, T., Washington, J., 2016. A North American and Global Survey of perfluoroalkyl substances in surface soils: distribution patterns and mode of occurrence. Chemosphere 161, 333–341.

Rayne, S., Forest, K., 2009. Perfluoroalkyl sulfonic and carboxylic acids: a critical review of physicochemical properties, levels and patterns in waters and wastewaters, and treatment methods. J. Environ. Sci. Health A 44 (12), 1145–1199.

Rosen, M.J., Kunjappu, J.T., 2012. Surfactants and Interfacial Phenomena. John Wiley and Sons, Hoboken, New Jersey.

Russo, A., Johnson, G.R., Schnaar, G., Brusseau, M.L., 2010. Nonideal transport of contaminants in heterogeneous porous media: 8. Characterizing and modeling asymptotic contaminant-elution tailing for several soils and aquifer sediments. Chemosphere 81, 366–371.

Silva, J.A.K., Simůnek, J., McCray, J.E., 2020. A modified HYDRUS model for simulating PFAS transport in the vadose zone. Water 12, 2758.

Van Glubt, S., Brusseau, M.L., Yan, N., Huang, D.D., Khan, N., Carroll, K.C., 2021. Column versus batch methods for measuring PFOS and PFOA sorption to geomedia. Environ. Pollut. 268, 115917.

Wang, Y., Khan, N., Huang, D., Carroll, K.C., Brusseau, M.L., 2021. Transport of PFOS in aquifer sediment: transport behavior and a distributed-sorption model. Sci. Total Environ. 779, 146444.

Weber, A.K., Barber, L.B., LeBlanc, D.R., Sunderland, E.M., Vecitis, C.D., 2017. Geochemical and hydrologic factors controlling subsurface transport of poly and perfluoroalkyl substances, Cape CodMassachusetts. Environ. Sci. Technol. 51, 4269–4279.

Xiao, F., Simcik, M.F., Halbach, T.R., Gulliver, J.S., 2015. Perfluorooctane sulfonate (PFOS) and perfluorooctanoate (PFOA) in soils and groundwater of a U.S. metropolitan area: migration and implications for human exposure. Water Res. 72, 64–74.

Yan, N., Ji, Y., Zhang, B., Zheng, X., Brusseau, M.L., 2020. Transport of GenX in saturated and unsaturated porous media. Environ. Sci. Technol. 54 (19), 11876–11885.

Zeng, J., Guo, B., 2021. Multidimensional simulation of PFAS transport and leaching in the vadose zone: impact of surfactant-induced flow and subsurface heterogeneities. Adv. Water Resour. 155, 104015.

Zeng, J., Brusseau, M.L., Guo, B., 2021. Model validation and analyses of parameter sensitivity and uncertainty for modeling long-term retention and leaching of PFAS in the vadose zone. J. Hydrol. 127172.